6th European Conference on Computational Mechanics (ECCM 6)
7th European Conference on Computational Fluid Dynamics (ECFD 7)
11–15 June 2018, Glasgow, UK

EXPERIMENTAL VALIDATION OF NUMERICAL APPROACH FOR FREE SURFACE FLOWS MODELLING BASED ON LATTICE BOLTZMANN METHOD

JAN VIMMR[1], LIBOR LOBOVSKÝ[1], ONDŘEJ BUBLÍK[1] AND TOMÁŠ MANDYS[1]

[1] NTIS - New Technologies for the Information Society, Faculty of Applied Sciences, University of West Bohemia
Univerzitní 8, 301 00 Plzeň, Czech Republic
jvimmr@kme.zcu.cz

Key words: Lattice Boltzmann Method, Volume of Fluid, Free Surface Flow, Gravity Casting, Experimental Measurement

Abstract. This study is focused on numerical as well as experimental investigation of free surface flows during gravity casting processes. The numerical simulations are based on an in-house implementation of the lattice Boltzmann method and results of the implemented algorithm are validated against the measured experimental data. In order to capture the free surface of an incompressible fluid, the algorithm based on the volume of fluid method is adopted. In addition, a surface tension term is included. The suggested computational algorithm is capable of capturing well an evolution of the free-surface flow during gravity casting as shown by comparison of results of the performed numerical simulations and experimental measurements.

1 INTRODUCTION

The free surface flow is a physical phenomenon involved in many manufacturing processes, e.g. material transport, machining, casting etc. Casting in particular involves flow of liquid or liquefied material into a rigid mold. Pouring the casting material into the mold can be driven by external pressure or by body force (e.g. gravity, centrifugal force). The latter aproach may be well employed in rapid prototyping, medical device molding, replacement part manufacturing, production of electronic devices, toys etc. The objective of the study is an analysis of free surface flow of the cast material inside a rigid mold during gravity casting while thermodynamic processes (such as heat transfer and solidification) are neglected.

Although there are earlier studies, mathematical and computational modelling of casting processes evolves rapidly since 1970s. A substantial development of computational tools arose in 1980s and 1990s when advanced mathematical models of complex physical properties were implemented. This includes finite difference and finite element solutions of non-isothermal flow of non-newtonian fluid [1, 2] or simulations of solidification in metal

casting [3]. Standard computational methods, such as finite element or finite volume method, are based on macroscopic description of continuum. The main drawback of these methods is the incompressibility constraint that requires solution of the Poisson equation. This leads to high computational demands and cumbersome parallelisation which is critical for the ability of solving problems when the mold geometry dimensions are large in comparison to the size of its most tiny topological structures.

The lattice Boltzmann method (LBM) models the macroscopic behaviour of the fluid using mesoscopic kinetic equations based on physics of microscopic processes [4, 5, 6]. Thus the LBM does not require solution of Poisson equation for incompressible flows and its implementation results in simple algorithm with low computational demands that is suitable for massive parallelisation [7].

Experimental investigation of real casting processes is challenging as the casting process often involves free surface flow of hot molten material inside a solid mold. In situ measurements of casting flow patterns can be performed using e.g. X-ray radiography and analysis of heat transfer between the liquid and the mold can be assessed using e.g. thermocouple wires. In situ analysis of aluminium casting may be found e.g. in [8, 9]. In order to provide an extensive data set measured under well controlled laboratory conditions, a water analogue model is often applied, such as in [10, 11]. In such cases, the mold can be made of transparent material such as polymethyl methacrylate (PMMA) which allows for analysis of flow patterns by means of standard optical measurement methods.

Within this study, a dedicated experimental test setup which enables execution of well-controlled benchmark tests is designed. These tests are then used for validation of an in-house computational algorithm based on the lattice Boltzmann method (LBM).

2 LATTICE BOLTZMANN METHOD

The lattice Boltzmann method (LBM) started to be very popular during the last decade [5, 6, 12]. The method is based on the mesoscopic fluid description unlike the classical methods that utilise the macroscopic description. Because of this approach, the LBM is simpler and less computationally demanding than the finite element and finite volume methods. The lattice Boltzmann method originates from the lattice gas cellular automata (LGCA), which represents a simplified molecular dynamics. Compared to the LGCA, the LBM operates with virtual particles which make it possible to solve various complex flow problems such as free surface flows and multiphase flows. To capture the free surface of an incompressible fluid, the algorithm based on the volume of fluid method (VOF) established by Thürey [13] is adopted in this study.

2.1 Discretisation

The LBM is based on the discretisation of the Boltzmann equation, which describes a time evolution of distribution function $f = f(\boldsymbol{x}, \boldsymbol{u}, t)$, $\boldsymbol{x} = [x_1, x_2, x_3]^T$, $\boldsymbol{u} = [u_1, u_2, u_3]^T$ in a phase space

$$\frac{\partial f}{\partial t} + \boldsymbol{u} \cdot \frac{\partial f}{\partial \boldsymbol{x}} = \Omega(f) \tag{1}$$

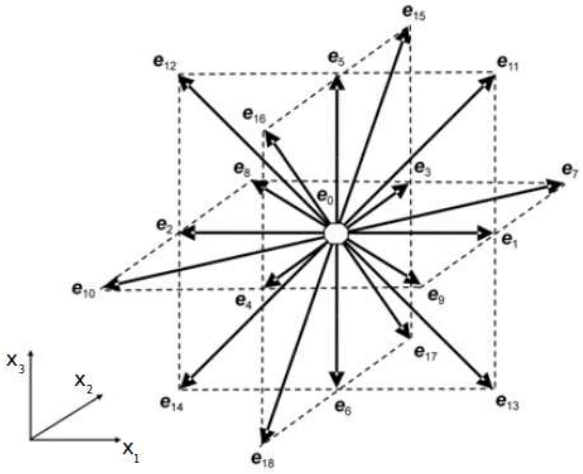

Figure 1: D3Q19 velocity model

where $\Omega(f)$ is the collision operator and external forces are neglected. The knowledge of the distribution function f permits the calculation of all macroscopic flow quantities.

First, the equation (1) have to be discretised in the velocity space while introducing the finite set of the velocity direction vectors $\boldsymbol{e}_\alpha$. This results in the discrete velocity Boltzmann equation

$$\frac{\partial f_\alpha}{\partial t} + \boldsymbol{e}_\alpha \cdot \frac{\partial f_\alpha}{\partial \boldsymbol{x}} = \Omega(f_\alpha) \tag{2}$$

After discretisation in the velocity space, the equation (2) is discretised in the physical space and time which yields a classical LBM scheme

$$f_\alpha(\boldsymbol{x} + \boldsymbol{e}_\alpha \Delta t, t + \Delta t) = f_\alpha(\boldsymbol{x}, t) - \boldsymbol{M}^{-1}\boldsymbol{S}(\tau)\boldsymbol{M}(f_\alpha - f_\alpha^{eq}) \tag{3}$$

where the convective scaling $\Delta \boldsymbol{x} = \boldsymbol{e}_\alpha \Delta t$ is introduced and f_α corresponds to the velocity direction vector $\boldsymbol{e}_\alpha$. In this study we consider the D3Q19 velocity model shown in Fig. 1, which defines the velocity direction vectors $\boldsymbol{e}_\alpha$ and the corresponding weights w_α.

The collision operator on the right hand side of equation (2) is approximated using the multiple relaxation time (MRT) operator [14], where $\boldsymbol{M}$ is the transformation matrix that projects f_α and f_α^{eq} into the discrete moment space $\boldsymbol{m} = [m_0, m_1, m_2, ..., m_{18}]^T$. The transformation matrix $\boldsymbol{M}$ is a linear mapping between the discrete velocity space and the discrete moment space $\boldsymbol{m}$, the diagonal matrix $\boldsymbol{S}$ contains the multiple relaxation times

$$\boldsymbol{S} = \mathrm{diag}(0, s_1, s_2, 0, s_4, 0, s_4, 0, s_4, s_9, s_{10}, s_9, s_{10}, s_{13}, s_{13}, s_{13}, s_{16}, s_{16}, s_{16}) \tag{4}$$

and the inverse matrix $\boldsymbol{M}^{-1}$ maps from the discrete moment space back to the discrete velocity space. The values of coefficients are $s_1 = 1.19$, $s_2 = s_{10} = 1.4$, $s_4 = 1.2$, $s_{16} = 1.98$. The remaining coefficients are related to the single relaxation time $s_9 = s_{13} = 1/\tau$. The equilibrium function f_α^{eq} is defined as [5]

$$f_\alpha^{eq}(\varrho, \boldsymbol{u}) = w_\alpha \varrho \left(1 + 3(\boldsymbol{e}_\alpha \cdot \boldsymbol{u}) + \frac{9}{2}(\boldsymbol{e}_\alpha \cdot \boldsymbol{u})^2 - \frac{3}{2}(\boldsymbol{u} \cdot \boldsymbol{u})\right) \tag{5}$$

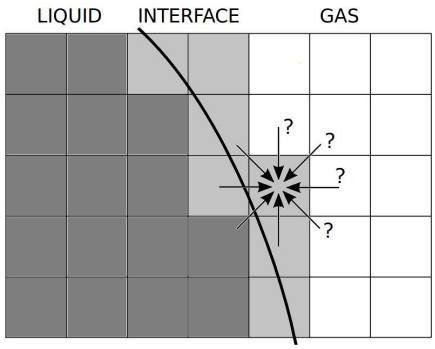

Figure 2: Liquid-gas interface, unknown values of functions f_α coming from the gas

Using Chapman-Enskog expansion can be shown, that the lattice Boltzmann method with this equilibrium function corresponds to the incompressible Navier-Stokes equations. The computation of the next time level $t + \Delta t$ using the LBM scheme (3) can be split into the following two steps:

- collision step, where the local values of distribution functions are computed

$$f_\alpha^c(\boldsymbol{x}, t) = f_\alpha(\boldsymbol{x}, t) - \boldsymbol{M}^{-1}\boldsymbol{S}(\tau)\boldsymbol{M}(f_\alpha(\boldsymbol{x}, t) - f_\alpha^{eq}) \tag{6}$$

- propagation step, where the local values of distribution functions $f_\alpha^c(\boldsymbol{x}, t)$ are propagated into neighbouring cells

$$f_\alpha(\boldsymbol{x} + \boldsymbol{e}_\alpha \Delta t, t + \Delta t) = f_\alpha^c(\boldsymbol{x}, t) \tag{7}$$

Since this work is focused on gravity casting processes, the external body force f_α^g is incorporated into a collision step as follows

$$f_\alpha^c(\boldsymbol{x}, t) = f_\alpha(\boldsymbol{x}, t) - \boldsymbol{M}^{-1}\boldsymbol{S}(\tau)\boldsymbol{M}(f_\alpha(\boldsymbol{x}, t) - f_\alpha^{eq}) + f_\alpha^g(\boldsymbol{x}, t) \tag{8}$$

where $f_\alpha^g(\boldsymbol{x}, t) = 3w_\alpha \varrho\, (\boldsymbol{e}_\alpha \cdot \boldsymbol{g})$ and $\boldsymbol{g}$ is the gravity acceleration.

2.2 Free surface modelling

The principle of free surface modelling with the lattice Boltzmann method was introduced in [13]. This approach is similar to the volume of fluid (VOF) method, with exception that the free surface is tracked with the help of the distribution functions f_α (corresponding to mass transfer in the α direction). The free surface modification of standard LBM algorithm distinguishes three types of cells, see Fig. 2:

- liquid (completely filled with liquid)
- gas (no liquid)
- interface (partly filled with liquid)

Due to the slight compressibility of the liquid, the mass m and the fluid fraction $\chi = m/\varrho$ have to be defined. Value of χ is equal to 1 for liquid, 0 for gas and $\chi \in (0,1)$ for the liquid-gas interface. The algorithm for free surface flow consists of basic steps described below. Firstly, the mass fluxes between the cells containing the liquid are computed as

$$\Delta m_\alpha(\boldsymbol{x}, t+\Delta t) = (f_{\bar{\alpha}}(\boldsymbol{x}+\boldsymbol{e}_\alpha \Delta t, t) - f_\alpha(\boldsymbol{x}, t)) \frac{\chi(\boldsymbol{x}+\boldsymbol{e}_\alpha \Delta t, t) + \chi(\boldsymbol{x}, t)}{2}$$

where $\bar{\alpha}$ denotes the opposite direction to α. The total cell mass change can be expressed as $m(\boldsymbol{x}, t+\Delta t) = m(\boldsymbol{x}, t) + \sum_\alpha \Delta m_\alpha(\boldsymbol{x}, t+\Delta t)$. After the mass change computation, the collision and propagation steps of the lattice Boltzmann method are performed. Then the microscopic variables are computed. Next the interface cell is changed into the liquid or the gas cell if

$$\begin{aligned} &m(\boldsymbol{x}, t+\Delta t) \geq \varrho(\boldsymbol{x}, t+\Delta t) \longrightarrow \text{liquid cell}, \\ &m(\boldsymbol{x}, t+\Delta t) \leq 0 \longrightarrow \text{gas cell}. \end{aligned}$$

Because the liquid and the gas cells cannot be next to each other, all liquid and gas cells adjacent to the cell with the changed state have to be switched into an interface cell. During the propagation step, the distribution functions $f_{\bar{\alpha}}(\boldsymbol{x}, t+\Delta t)$ coming from the gas cells to an interface cell are unknown and have to be reconstructed, see Fig. 2. The reconstruction is performed using the equilibrium function, where ϱ_a corresponds to an external pressure $\varrho_a = 3(p_a + 2\kappa\sigma)$ and $\boldsymbol{u}$ is the interface velocity

$$f_{\bar{\alpha}}(\boldsymbol{x}, t+\Delta t) = f^{eq}_\alpha(\varrho_a, \boldsymbol{u}) + f^{eq}_{\bar{\alpha}}(\varrho_a, \boldsymbol{u}) - f_\alpha(\boldsymbol{x}, t)$$

Term $2\kappa\sigma$ corresponds to the surface tension, where $\kappa = \nabla \cdot \frac{\nabla\chi}{|\nabla\chi|}$ is surface curvature and σ is coefficient of surface tension. The algorithm is described in detail in [13].

2.3 Units conversion

Macroscopic flow quantities in lattice Boltzmann units are computed as

$$\varrho = \sum_\alpha f_\alpha, \quad \varrho\boldsymbol{u} = \sum_\alpha f_\alpha \boldsymbol{e}_\alpha, \quad p = \frac{1}{3}\varrho$$

The values of macroscopic flow variables are expressed in lattice Boltzmann units in LBM simulations. In order to get physical values of flow variables, the conversion between lattice Boltzmann units and physical units have to be established. When using the lattice Boltzmann equation, the physical character of the fluid flow is described by only one parameter τ. Let H denote an arbitrary physical characteristic dimension of computational geometry and n denote the number of lattices corresponding to characteristic dimension H. Let u_{real} denote the expected maximal value of physical velocity. For stability reasons, the maximal velocity in lattice Boltzmann units is set to $u_{LB} = 0.1$. The last required

parameter is physical value of kinematic viscosity ν. Using the listed values, the following space and velocity ratios are defined as

$$C_H = \frac{H}{n}, \quad C_U = \frac{u_{real}}{u_{LB}} \tag{9}$$

The ratios for other variables between physical and lattice Boltzmann units are derived using C_H and C_U

$$C_T = \frac{C_H}{C_U}, \quad C_P = \frac{1}{3}C_U^2, \quad C_\nu = \frac{C_H^2}{C_T}, \quad C_F = \frac{C_H}{C_T^2}, \quad C_{ST} = \frac{C_H^3}{C_T^2}$$

where C_T is the time ratio, C_P is the pressure ratio, C_ν is the kinematic viscosity ratio, C_F is the force ratio and C_{ST} is the surface tension ratio. The kinematic viscosity in lattice Boltzmann units ν_{LB} and the relaxation parameter τ can be expressed as

$$\nu_{LB} = \frac{\nu}{C_\nu}, \quad \tau = \frac{1}{2} + 3\nu_{LB} \tag{10}$$

The physical value of computational time can be expressed as $T = C_T\, n_{iter}$, where n_{iter} is a number of the time iteration.

3 NUMERICAL AND EXPERIMENTAL MODELLING

The gravity casting flow was investigated both numerically and experimentally. The performed experiments were designed so that they provided data for validation of the implemented LBM algorithm. Two gravity casting flow scenarios were considered. Firstly, a propagation of the cast material inside a long horizontal channel was studied, the setup geometry is displayed in Fig. 3 (right). Secondly, a gravity flow inside a complex vertical labyrinth, shown in Fig. 3 (left), was analysed. In both cases, the numerical results of LBM simulations were confronted qualitatively as well as quantitatively with results of the executed experimental measurements.

A special attention was paid to propagation of the fluid along the channel length and to the free surface shape evolution. Heat transfer as well as solidification of the cast material were not a subject of this study.

Each test case was performed for one of the selected Newtonian viscous fluids at standard room temperature. These fluids and their physical properties are listed in Table 1. The viscosity, the surface tension and the density of the test fluids were precisely measured both for fresh unused samples (i.e. before the casting experiments) and for samples of fluid that were already cast inside the mold (i.e. after the execution of casting experiments).

3.1 Horizontal channel

The first test case aimed at a direct comparison of the numerical and experimental data in terms of propagation of the cast material in a simple geometry, ideally in a long horizontal channel with a single inlet at one end and a single outlet at the other end.

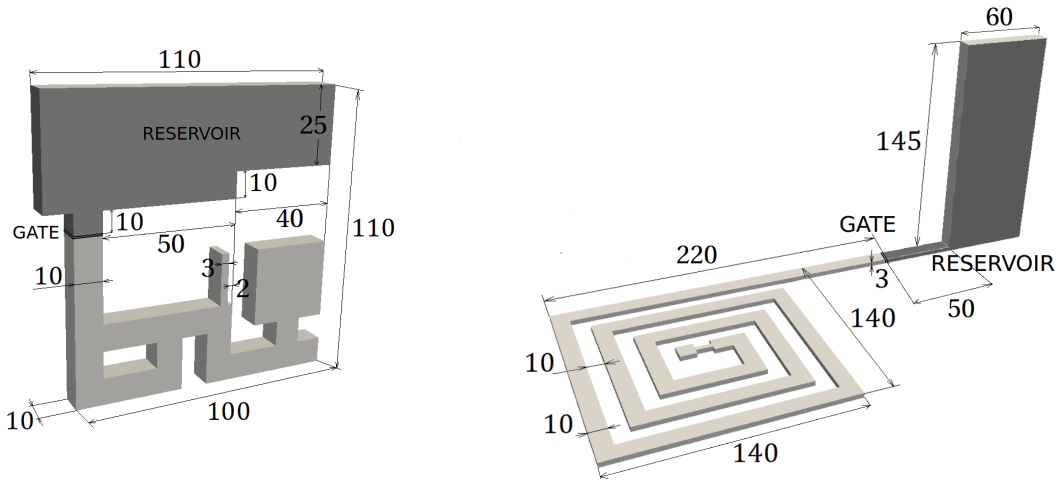

Figure 3: Geometry of vertical (left) and horizontal (right) setup of the gravity casting test cases with dimensions expressed in [mm]

Table 1: Parameters of the test liquids

	Sugar solution	Glycerol solution
density ϱ [kg/m^3]	1244	1260
dynamic viscosity η [mPa $\cdot$ s]	41.6	640
surface tension σ [mN/m]	46	63

In order to fit the experimental setup within a square field of view, a spiral shape channel was selected as depicted in Fig. 3 (right).

The test setup geometry consisted of two connected parts, a vertical reservoir and a horizontal mold. The reservoir holded 90 ml of liquid material (sugar solution in this case) which was cast under gravity into the horizontal channel of rectangular cross-section. The cross-section did not vary along the channel length and its dimensions were 3 mm $\times$ 10 mm, where 3 mm was the height of the channel. In longitudinal direction, the horizontal channel winded in a 1160 mm long spiral.

The experimental stand was designed so that the propagation of the material in a mold could be analysed using standard optical methods. Both the vertical reservoir as well as the horizontal channel were milled in transparent PMMA sheets. The reservoir and the channel were separated by a removable gate. The gate was designed so that it initially obstructed the horizontal channel (thus it holded the test liquid inside the reservoir before the start of the experiment), but it was free to slide in vertical direction. At the beginning of each measurement, the gate was removed abrubtly (the gate removal time was less than 1/60 s) and the liquid flew freely into the rigid channel. The fluid flow was driven solely by gravity.

Overall 10 runs of gravity casting experiments were executed. A qualitative comparison of a randomly selected experimental run with results of LBM simulation is shown

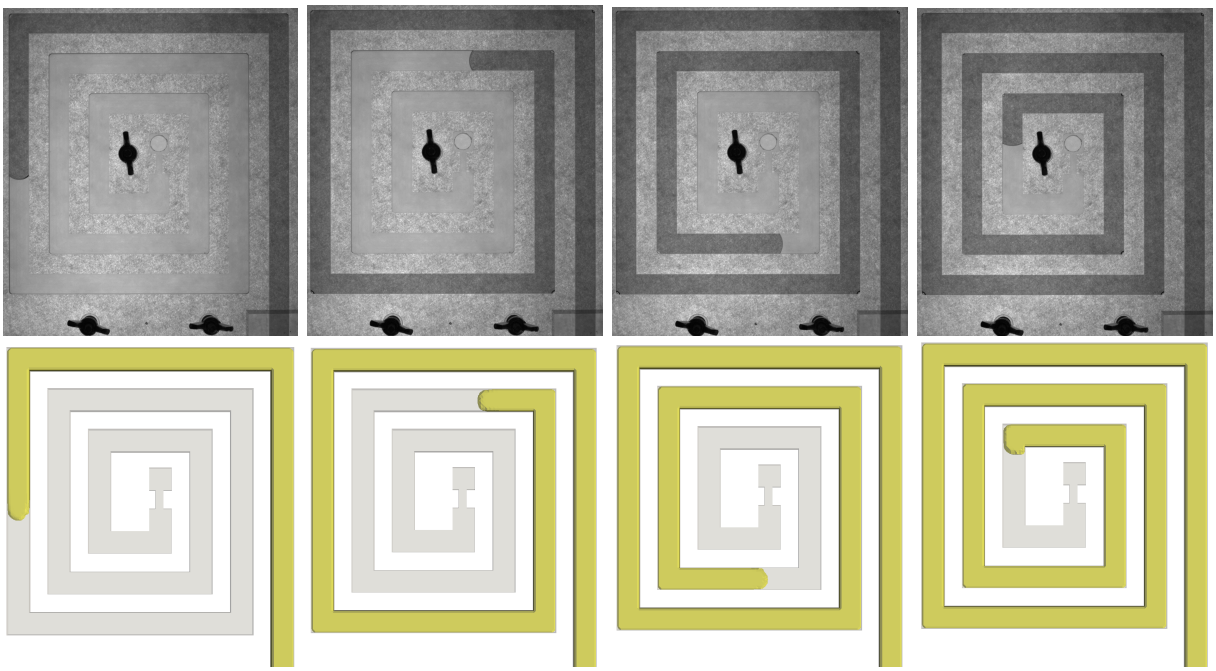

Figure 4: Top view of the horizontal channel: experimental data (top) vs. numerical results (bottom) at time 5, 15, 25 and 35 s

in Fig. 4. Although a satisfactory agreement between experiments and numerical data can be observed, the presented images indicate that the propagation of the wave front as computed by LBM gets slightly delayed behind the experimental results. This observation is confirmed in Fig. 5 (right), which displays a position of the wave front along the horizontal channel centerline (in terms of a distance from the gate) vs. time. The channel centerline is indicated as a blue curve in Fig. 5 (left). It is obvious that the wave front propagation as computed by the LBM algorithm corresponds well to the measured data in the first phase of the casting process while it gets sloved down later on. Nevertheless, the numerically predicted duration of the entire casting process (by means of LBM) is about the same as the duration of the slowest experimental run.

The slight difference in time evolution of the wave front propagation between numerical and experimental results may be attributed to several factors. Probably the major factor is the gate removal. In the experiments, during the gate removal the gate slides vertically while the horizontal channel opens gradually in non-zero time. This process is not modelled in the numerical simulations, where the gate removal happens in zero time and the horizontal channel is opened at once.

A second key factor is a limited accuracy of measurements of the test fluid physical properties. Although the test fluid is considered to be Newtonian, its rheological measurements show a decreasing tendency of the dynamic viscosity value with the decreasing shear rate. This was not reflected in the numerical simulation, where a constant viscosity value was employed. This constant was determined as an average of all the viscosity measurements for all samples within a reasonable range of shear rates. Its value might be slightly

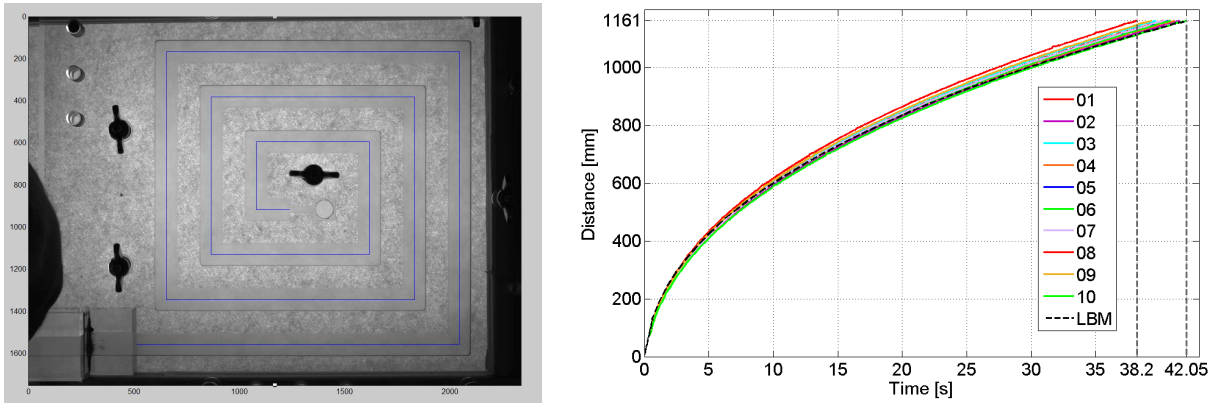

Figure 5: Propagation of the wave front along the centerline of the horizontal channel

overestimated since an absolute measurement of the dynamic viscosity at extremely low shear rates was not possible.

Some minor role on wave front propagation in the experiments may be also played by precision of mold machining in terms of surface smoothness and precision of experimental setup assembly. However these factors are considered negligible.

3.2 Vertical labyrinth

In the second test case, a free surface flow in a gravity casting mold of rather complex vertically oriented geometry was analysed. It was a labyrinth of channels, as displayed in Fig. 3 (left). In this case, the reservoir of cast material was positioned right above the labyrinth of channels and was filled with 35.5 ml of liquid material (glycerol solution). The labyrinth channels had a square cross-section 10×10 mm except for the venting channel in the central part which cross-section was rectangular $3\,\text{mm} \times 10\,\text{mm}$, see Fig. 3 (left). At the end of the labyrinth, the channel opened to a $30\,\text{mm} \times 30\,\text{mm} \times 10\,\text{mm}$ large chamber. The reservoir and the labyrinth were separated by a horizontal gate. Using this setup, the gate removal took less than 1/30 s. The setup geometry (i.e. the reservoir and the labyrinth of channels) was milled in transparent PMMA sheets. In this case, series of overall 30 experimental runs were executed. A brief summary of their results is provided below.

After the gate removal, the cast material experienced a free fall before it hit the bottom of the labyrinth and spread into its horizontal and vertical channels, see Fig. 6. The free falling highly viscous liquid formed a neck which formation was strongly influenced by the gate removal. The gate removal process was optimised so that the neck was centered within the inlet vertical channel. The vertical labyrinth was designed so that the air did not get entrapped in the labyrinth, except for the large bubbles in the inlet vertical channel which formed after the initial neck of fluid hit the labyrinth bottom and consequently filled the lower part of the vertical channel.

In general, the gravity flow in this vertical labyrinth resulted in a more complex free surface flow then in the case of horizontal channel. This included not only an interaction

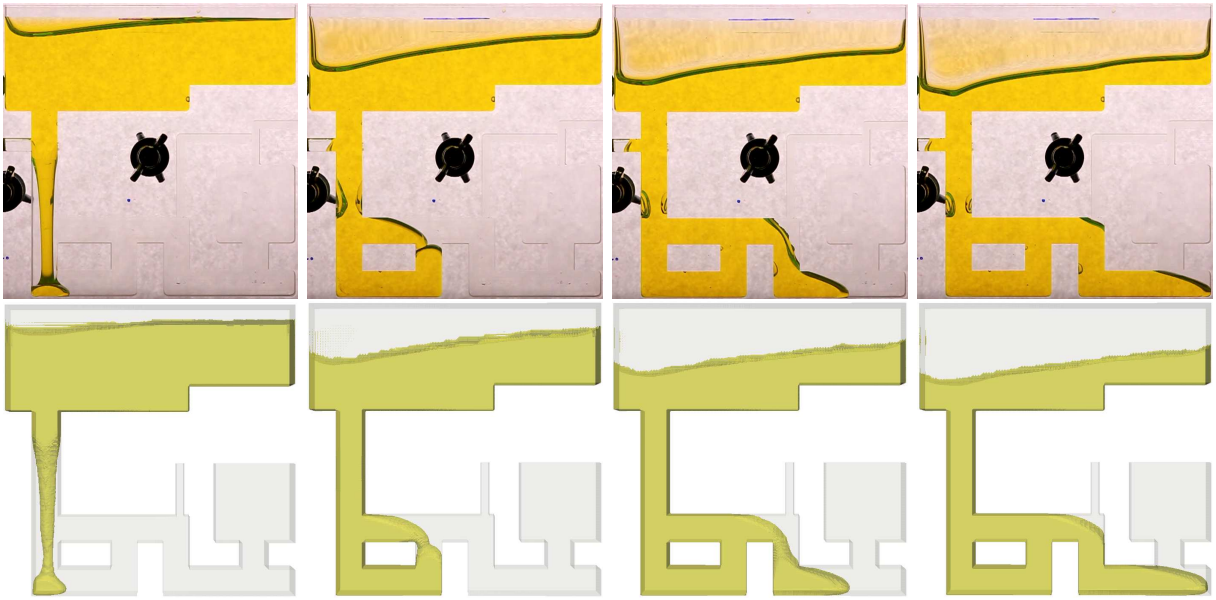

Figure 6: Vertical labyrinth: experimental data (top) vs. numerical results (bottom) at time 0.20, 1.08, 2.18 and 2.88 s

between fluid and rigid walls but also an interaction of free surface interfaces which merged together. Nevertheless, a qualitative comparison displayed in Fig. 6 reveals a reasonable agreement between experimental measurements and numerical results of the implemented LBM algorithm.

A quantitative comparison of experiments and simulations is displayed in Fig. 7 (right), which provides a plot of wave front arrival times at 7 selected locations. These locations are marked in Fig. 7 (left). The locations are numbered correspondingly to the propagation of the test fluid in the labyrinth. From the plotted data, it is obvious that the uncertainity level of the experimental results increases with the increasing number of location. However, the mean values of the experimental arrival times are in reasonable agreement with the LBM results.

Also for the vertical labyrinth, there are the same factors that influence the comparison of experimental and numerical data as in the previous test case of the horizontal channel flow. In addition, large variation in experimental data themselves is introduced by the design of the vertical labyrinth and its gate release mechanism. The key source of uncertainity in the experimental data is the gate removal and the subsequent vertical flow of the test fluid. The gate slides in a horizontal direction and the shape of vertically falling fluid's free surface strongly depends on the duration of the gate removal. On the contrary, the presented LBM simulation does not include a model for the moving gate.

4 CONCLUSIONS

The numerical results obtained using the in-house LBM code showed a reasonable agreement with the assessed experimental data. The experimental measurements of the gravity casting flow inside the long horizontal channel provided a set of data for validation

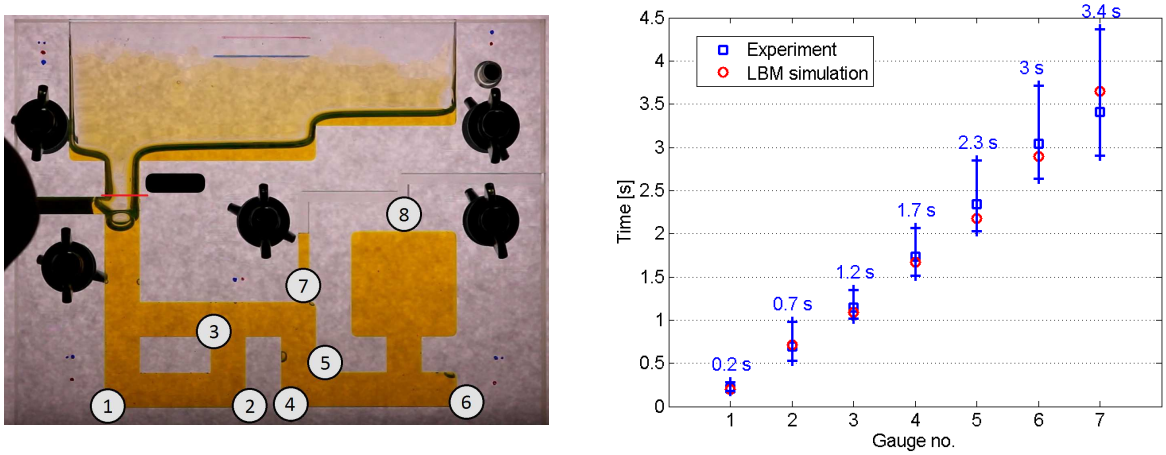

Figure 7: Vertical labyrinth: comparison of wave arrival times at selected locations

of the implemented LBM algorithm. Despite the significant uncertainity of the experimental measurements of the gravity casting in the vertical labyrinth, the LBM simulations of this test case were capable of capturing the complex flow properties both qualitatively and quantitatively, provided a large set of experimental measurements was carried out. The simplicity of the LBM and its ability to simulate complex flow problems efficiently makes this method suitable for simulation of real world casting problems.

5 ACKNOWLEDGEMENT

The authors appreciate the kind support by the grant GA 18-25734S "Experimental and computational modelling of free surface flow of non-Newtonian fluids with dispersed particles" of the Czech Science Foundation.

REFERENCES

[1] Hieber, C.A. and Shen, S.F. A finite-element/finite-difference simulation of the injection-molding filling process. *J. Nonnewton. Fluid Mech.* (1980) **7**:1–32.

[2] Lee, C.C., Folgar, F. and Tucker, C.L. Simulation of compression molding for fiber-reinforced thermosetting polymers. *J. Eng. Ind.* (1984) **106**:114–125.

[3] Lewis, T.B. and Nielsen, L.E. Dynamic mechanical properties of particulate-filled composites. *J. Appl. Polym. Sci.* (1970) **14**:1449–1471.

[4] Chen, S. and Doolen, G. D. Lattice Boltzmann method for fluid flows. *Annu. Rev. Fluid Mech.* (1998) **30**:329–364.

[5] Succi, S., Benzi, R. and Higuera, F. The lattice-Boltzmann equation a new tool for computational fluid dynamics. *Physica D* (1991) **47**:219–230.

[6] Sukop, M., Thorne, C. and Daniel Jr., T. *Lattice Boltzmann Modeling. An Introduction for Geoscientists and Engineers*. Springer-Verlag Berlin Heidelberg, 2007.

[7] Calore, E., Gabbana, A., Kraus, J., Pellegrini, E., Schifano, S.F. and Tripiccione, R. Massively parallel lattice-Boltzmann codes on large GPU clusters. *Parallel Comput.* (2016) **58**:1–24.

[8] Sirrell, B., Holliday, M. and Campbell, J. Benchmark testing the flow and solidification modeling of Al castings. *JOM* (1996) **48**:20–23.

[9] Zhao, H., Ohnaka, I. and Zhu, J. Modeling of mold filling of Al gravity casting and validation with X-ray in-situ observation. *Appl. Math. Model.* (2008) **32**:185-194.

[10] Ha, J., Cleary, P., Ahuja, V. and Nguyen, T. Simulation of die filling in gravity die casting using SPH and MAGMAsoft. *Proc. 2nd International Conference on CFD in the Minerals and Process Industries*, CSIRO, Melbourne, Australia, 1999, pp. 423–428.

[11] Kowalewski, T.A., Cybulski, A. and Sobiecki, T. Experimental model for casting problems. *Computational Methods and Experimental Measurements X, WIT Transactions on Modelling and Simulation* (2001) **30**:179–188.

[12] Ginzburg, I. and Steiner, K. Lattice Boltzmann model for free-surface flow and its application to filling process in casting. *J. Comput. Phys.* (2003) **185**:61–99.

[13] Thürey, N. *Physically based Animation of Free Surface Flows with the Lattice Boltzmann Method*. Doctoral thesis, Erlangen, 2007.

[14] d'Humières, D. Multiple-relaxation-time lattice Boltzmann models in three dimensions. *Philos. Trans. A Math. Phys. Eng. Sci.* (2002) **360**:437–451.